“Fabrication and Optical Properties of Decorated Silicon Nanowires”

M.Sc. Thesis

By

Pooja Yadav

DISCIPLINE OF PHYSICS

INDIAN INSTITUTE OF TECHNOLOGY INDORE

JULY 2016

“Fabrication and Optical Properties of Decorated Silicon Nanowires”

A THESIS

Submitted in partial fulfillment of the
requirements for the award of the degree
of
Master of Science

by

Pooja Yadav

DISCIPLINE OF PHYSICS
INDIAN INSTITUTE OF TECHNOLOGY INDORE
JULY 2016

INDIAN INSTITUTE OF TECHNOLOGY INDORE

CANDIDATE'S DECLARATION

I hereby certify that the work which is being presented in the thesis entitled **"Fabrication and Optical Properties of Decorated Silicon Nanowires"** in the partial fulfillment of the requirements for the award of the degree of **MASTER OF SCIENCE** and submitted in the **DISCIPLINE OF PHYSICS, Indian Institute of Technology Indore**, is an authentic record of my own work carried out during the time period from July 2015 to July 2016 under the supervision of Dr. Rajesh Kumar associate professor, Indian Institute of Technology Indore and Dr. P.R. Sagdeo, associate professor, Indian Institute of Technology Indore**.**

The matter presented in this thesis has not been submitted by me for the award of any other degree of this or any other institute.

Signature of the student with date

(Pooja Yadav)

This is to certify that the above statement made by the candidate is correct to the best of our knowledge.

Signature of the Supervisor #1

Dr. Rajesh Kumar

Signature of the Supervisor #2

Dr. Pankaj R. Sagdeo

Pooja Yadav has successfully given her M.Sc. Oral Examination held on 27th June, 2016

Signature(s) of Supervisor(s) of MSc thesis
Date:

Convener, DPGC
Date:

Signature of PSPC Member #1
Date:

Signature of PSPC Member #2
Date:

ACKNOWLEDGEMENT

I wish to thank my supervisors Dr. Rajesh Kumar and Dr. P.R. Sagdeo for their valuable guidance, useful comments and remarks.

I am highly thankful to my bhaiya Dr. Shailendra Saxena for his spontaneous support and his valuable lessons that will help me throughout my academic career.

I would also like to thank the PSPC members Dr. Preeti Bhobe and Dr Sanjay Singh.

I am obliged to all my semiconducting and material research laboratory seniors, and collegues Preetam Singh and Haardik Pandey for keeping the environment energetic. The happy moments we shared from lab will be remembered forever.

I also acknowledge all my batch mates for giving me long lasting memories and continuous help in course work, seminars, projects etc.

I am highly thankful to Sophisticated Instrumentation Centre (SIC) at IIT Indore for Photoluminescence and SEM measurements. Without their support this report would not have been possible.

Partial financial support from Department of Science and Technology (DST), Govt. of India is acknowledged.

Pooja Yadav
M.Sc. II Year
Discipline of Physics
IIT Indore

DEDICATED TO

MY PARENT AND TEACHERS

Abstract

Well aligned Silicon Nanowires (SiNWs) are successfully fabricated by metal induced etching (MIE) technique. Role of Silver nanoparticles (AgNPs) on the porosification of Silicon has also been studied. SEM images confirm the nanostructures formed in the sample. Photoluminescence (PL) has been carried out to see quantum confinement effect in SiNWs samples. Further effect of metal nanoparticle decoration on SiNWs is studied. EDS spectroscopy confirmed the presence of MNPs on SiNWs. A significant shift in the PL energy is observed after decoration. An appreciable enhancement in absorption spectra of decorated SiNWs observed which has potential to be used in solar cell applications for light trapping purpose.

LIST OF PUBLICATIONS

1. Shailendra K. Saxena, Priyanka Yogi, **Pooja Yadav**, Suryakant Mishra, Haardik Pandey, Hari Mohan Rai, Vivek Kumar, Pankaj R. Sagdeo, Rajesh Kumar, Role of metal nanoparticles on porosification of silicon by metal induced etching (MIE), Superlattices and Microstructures, 94,101-107, (2016).

TABLE OF CONTENTS

LIST OF FIGURES

LIST OF TABLES

ACRONYMS

Acronym	**Meaning**
NSs	Nanostructures
SiNSs	Silicon Nanostructures
SiNWs	Silicon Nanowires
D-SiNWs	Decorated Silicon Nanowires
PL	Photoluminescence
VLS	Vapour Liquid Solid
DRA	Diffused Reflectance Analysis
MNPs	Metal Nano-Particles
MIE	Metal Induced Etching
FE-SEM	Field Emission Scanning Electron Microscope
IPA	Isopropyl Alcohol
PS	Porous Silicon
CIF	Centre for Instrumentation Facility
SIC	Sophisticated Instrument Centre
SE1	Secondary Electrons
SE2	Backscattered Electrons
SE3	Electrons not from sample

Chapter 1

Introduction

Nanoscience and nanotechnology are recent developments of science and engineering which are developing at very fast pace. Such developments demand the fabrication of novel nanomaterials having improved properties over traditional materials in order to miniaturize the device dimensions. Moreover, these materials should have potential to be applied in areas of physical, chemical, biological sciences and in other interdisciplinary fields of engineering and science. Nanoparticles are an assembly of number of molecules and atoms bonded together which are intermediate in size between individual atoms and bulk materials. As these nanoparticles are larger than atoms and smaller than bulk materials therefore their properties lies between macroscopic solid and atomic system. The major factors that are responsible for these change are 1) High surface to volume ratio 2) Quantum confinement effect and 3) Electrodynamics interactions[1–4].

Synthesis and applications of semiconducting nanostructures (NSs) are currently intense subject of research. These nanostructures offer a wide range of opportunities for new generation of nanoscale photovoltaic and optical devices. In fact, interest in the NSs is triggered by their distinguished physical, electronic, optical and thermodynamical properties from their corresponding bulk materials which can be attributed to the quantum confinement effect. As quantum confinement brings uniqueness in properties, as have been mentioned earlier.

Now, silicon being a leading semiconducting material is dominating current semiconductor industry until now. Silicon nanomaterials are the most important type of nanomaterials featuring unique merits such as optical, electronical and mechanical properties. More importantly, Silicon exists in human as a common trace element. So the biocompatibility of silicon leads silicon nanomaterials based applications non-hazardous and environmental friendly for the society.

Silicon Nanostructures (SiNSs) are one of the most promising materials for current semiconducting industry and are well-documented as promising building blocks for devices in the fields of nanoelectronics, optoelectronics, energy conversion, energy storage and sensors[5]. Extensive studies on silicon thin films, nanowires, nanoparticles, nanotubes and porous structures have been carried out over past few decades due to their unique physical, catalytic and various other properties. In this project, work has been done on porous silicon nanowires (SiNWs) which are one dimensional structure that are confined in two directions and has one degree of freedom i.e. motion only in one direction. Moreover large surface area and high charge collection efficiency makes the SiNWs different from other NSs which makes it more useful.

There are two approaches to fabricate SiNWs viz. bottom up and top down. Bottom up processes can be defined as those where structures are assembled from components in additive fashion. Top down fabrication strategies use etching to carve structures from larger piece of material in subtractive manner. Sometimes requirement of significant demand depends on mode of fabrication[6,7].

Several bottom up methods such as vapor liquid solid (VLS) by chemical vapor deposition, molecular beam epitaxy, laser ablation, thermal evaporation have been successfully developed for the systematic fabrication of SiNWs. Top down approaches are recently developed which include ion etching, electrochemical etching and metal induced chemical etching methods. Metal induced chemical etching method is easy, low cost, solution beaker process that enables formation of vertically aligned SiNWs array over wafer scale[8].

Fabricated SiNSs can be characterized by various techniques like Field effect scanning electron microscopy (FESEM), Photoluminescence (PL), Diffuse reflectance analysis (DRA), Raman spectroscopy etc. FESEM is used to study surface topology, morphology and approximate size estimation of SiNSs. DRA is used to investigate the band gap and absorption spectra while PL for emission spectra.

Crystalline Silicon (c-Si) is an indirect bandgap semiconductor which limits it as a poor emitter of light. Light emission in c-Si is phonon mediated with low intensity emission in the near infrared region. The competitive non radiative recombination rates in c-Si are much higher than radiative ones and most of electron hole pairs recombine non-radiatively giving no strong color effects. When size of silicon is reduced to nanoscale the overlap of electron–hole wave functions increased, leading to enhancement of recombination rate of carriers. As a result, small sized SiNSs show strong fluorescence, showing long awaited optical applications. Si NSs show efficient photoluminescence in the visible to near IR range when excited by radiation. The PL may originate from electron-hole pair created by incident light[9] or may be by luminescent defect centers[10]. Both mechanism compete each other and can be achieve within same nanostructure[11]. Along with dependency on size, the origin of PL depends on method of synthesis also.

Now a days hybrid nanomaterial i.e. nanohybrides that combine the various types of nanostructures like nanoparticles, nanowires, nano rods etc. have also gained lot of attention[12–14]. Moreover, to meet the increasing demands of various applications, nanohybrides with multifunctional properties have been fabricated by combinations of various functional nanostructures. In recent years, silicon based nanohybrides include SiNSs decorated with metal nanoparticles (MNPs) like AuNPs, AgNPs, PtNPs etc or with magnetic materials like Mn, Fe, Fe_2O_3 etc. These have developed better utilization and performance in catalytic reactions, biological sensors, bioimaging, surface enhanced resonance spectroscopy (SERS) and cancer therapies etc[4,15–17]. Basically noble metals like Pt, Au, Ag ions can be facilely reduced by surface covered Si-H bonds of SiNWs, yielding Pt, Au, Ag decorated SiNWs. Such resultant metal decorated nanostructures (D-NSs) have extensively studied.

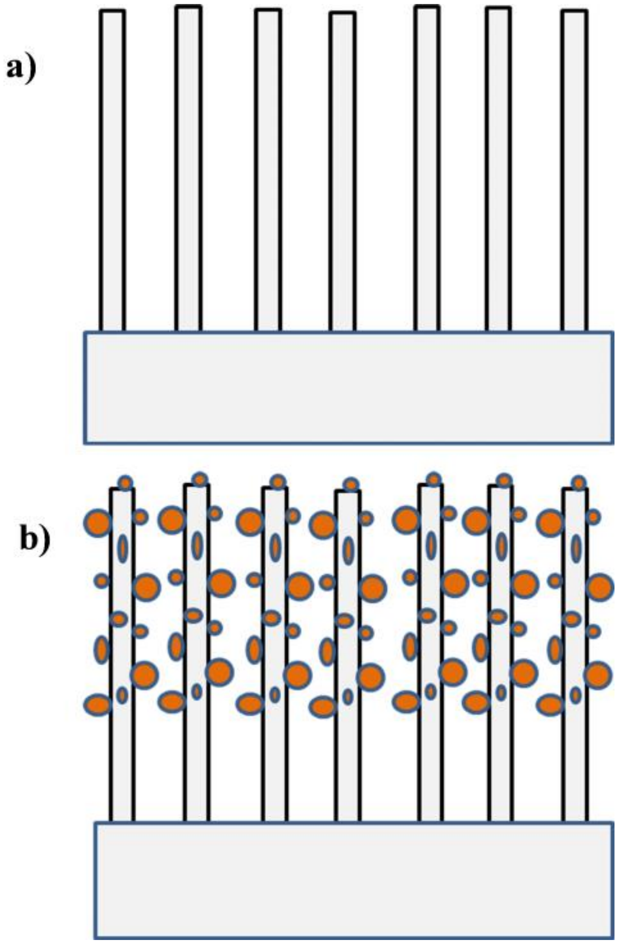

Fig. 1.1: Schematic diagram of a) SiNWs and b) D-SiNWs

Survey shows that after decoration with Ag metal nanoparticles on porous SiNWs, PL intensity enhancement of seven folds has been reported[18]. While Gold nanoparticles increase the PL brightness by a factor of five[19]. Such good enhancement in luminescence and bright emission is very useful in sensor based applications.

UV-Vis spectroscopy is based on the principle of electronic transition in atoms or molecules upon absorbing suitable energy from an incident light that allows electrons to excite from a lower energy state to higher excited energy state. While interaction with infrared light causes molecules to undergo vibrational transitions, the shorter wavelength with higher energy radiations in the UV (200-400 nm) and Visible (400-800 nm) range of the electromagnetic spectrum causes many atoms/molecules to undergo electronic transitions. Bulk silicon starts absorbing the light from 1.1eV which changes when it enters into nano region. In addition to this it has been observed that, when size is reduced, band gap enhancement is seen in silicon NSs due to quantum confinement effect.

Now, enormous utilization of solar energy is recognized due to shortage of fossil fuels[20–22] and great effort is being devoted for developing solar energy conversion systems. Literature survey shows that SiNSs arrays can significantly suppress light reflection across a broad spectrum and serve as antireflection coating for Si solar cell applications.

Over 50 years, commercial silicon photovoltaic has been developed to convert sunlight into electricity at efficiency of 20% and displaces nonrenewable power consumed[23]. Silicon photovoltaic cells using silicon wafer requires extensive purification to maintain reasonable performance[24,25]. Using solar cells with nanostructured radial p-n junctions may solve these problems by allowing improved light scattering and trapping[26] and has provided 10 times efficiency improvement over thin silicon absorber films. SiNWs increase the path length of light and gives better absorption than thin films[27].

Aside from excellent light absorption and efficient radial charge collection, SiNWs have direct 1D electronic pathways allowing for 1D transport of charge carriers along the length of every wire. Efficiency reported from SiNWs based solar cells is 7 to 8% of the required practical applications. As prepared SiNWs gives large surface area and high charge collection ability still suffers from various junction problems which imposes a major barrier to achieve efficient solar cells[28]. Thus further efficiency improvement is much needed.

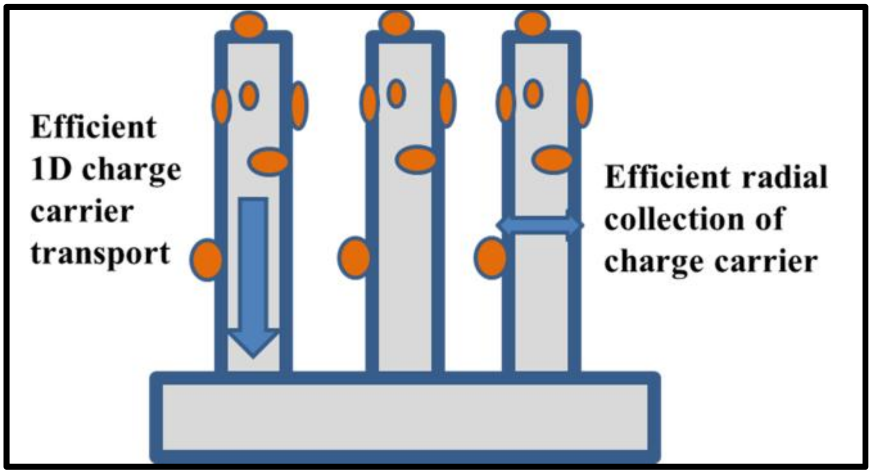

Fig. 1.2: 1D carrier transport and charge collection of SiNWs

To improve the absorption and emission properties as well as prevention of SiNWs from environmental degradation i.e. conversion into SiO_2 can be effectively prohibited using metal decoration. Decoration of discrete semiconductor or metallic nanoparticles on carbon nanotube[29,30] and ZnO nanostructures[19] can yield a significant enhancement in photo conversion which has been already employed by many research groups. So, similar enhancement may be anticipated when MNPs most preferably noble MNPs are deposited on SiNWs. Pt NPs decorated SiNWs yielded significant enhancement in solar energy conversion efficiency upto 8.1% which is highest ever reported for SiNWs solar cells, demonstrating them to be promising hybrid system for efficient solar energy conversion[28]. In addition to emission efficiency improvement these MNPs can also prevent degradation of Si NWs, thereby prohibiting the oxide formation.

Summary of the project work:

SiNWs, one of the most celebrated silicon nanostructures have been fabricated by MIE method. The process of SiNWs formation using MIE incorporate two steps i.e. i) deposition of metal NPs on silicon wafer and then ii) etching of samples. The morphology and structures of the as-prepared Porous SiNWs were further studied by FESEM. Porous structures from top view and well aligned, dense SiNWs from vertical side are viewed. Further emission and absorption spectra have been systematically investigated using PL and DRA spectroscopies respectively. PL ensures the conversion from indirect band gap of silicon to direct band gap of SiNWs with a broad emission peak centered mainly at 600 nm. Resulting PL spectra of SiNWs has started to show the strong color effects after coming into visible region. DRA gives the absorption spectra and determines the band gap of SiNWs. The PL spectra and band gap measured from DRA are in good agreement with each other which signifies the involvement of quantum confinement effect occurring in porous SiNWs. SiNWs are then decorated with Au and Pt MNPs. Presence of MNPs on SiNWs is confirmed by EDS spectroscopy. Again the PL and DRA spectra of D-SiNWs are studied which shows significant enhancement in intensities and a significant shift in the peak energies of both. The change in spectra of D-SiNWs depends on characteristics of MNPs like shape, size, electron density, dielectric constant etc. those can be varied according to desire. The work done in this project has immense potential for the development of SiNWs based optoelectronic devices and materials.

Chapter 2

Theoretical Background

2.1 Silicon and its structure

Semiconductor materials have been at the center of condensed matter physics research for many decades, and this situation has not changed up to the present day. As a multi-billion dollar semiconductor industry demands for better performance of their devices, physicists and material scientists work diligently to satisfy the demand. New materials rise to the spotlight while the properties of old ones become better known. The position of silicon as the major semiconductor material has not yet been shaken.

Silicon is eighth most found element in universe by mass but it is not found in its pure element. It is distributed as dust, sand, planetoids in the form of silicon dioxide and silicates. Over 90% of earth crust is composed of silicate materials making silicate the second most abundant element on earth after oxygen. Naturally occurring silicon is composed of three stable isotopes, silicon-28, silicon-29, and silicon-30, with silicon-28 being the most abundant (92% natural abundance). Because silicon is an important element in semiconductors and high-technology devices, many places in the world bear its name. For example, Silicon Valley in California, bears the element's name since it is the base for a number of computer technology related industries.

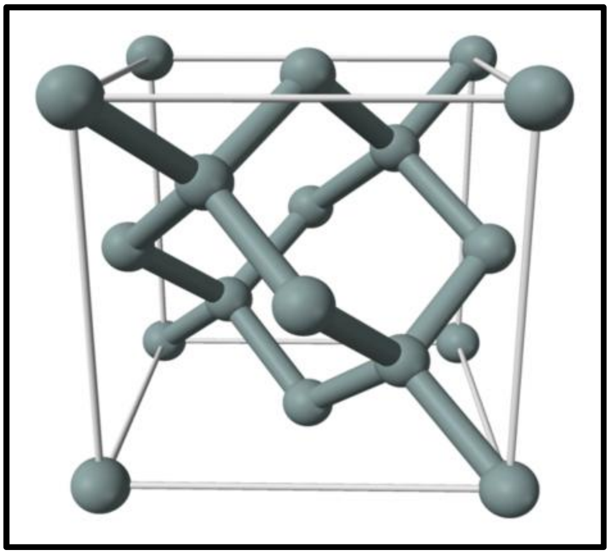

Fig. 2.1 Crystal structure of silicon

In the crystalline form, pure silicon has gray color and metallic luster. Silicon has atomic number Z=14 with 1s, 2s, 2p, 3s fully filled subshell and 4 valence electrons in 3p subshell. The crystalline silicon (c-Si) has diamond type structure consisting of two interpenetrating face centered cubic (FCC) lattices, displaced along the body diagonal of the cubic cell by one-fourth of the diagonal length. It is regarded as an FCC lattice with a basis containing two identical atoms. In crystalline silicon structure (c-Si), each Si atom is connected to four other atoms tetrahedrally. The lattice parameter of c-Si is a=0.543 nm and tetrahedral angle of 109.20. Silicon is semiconductor with indirect band gap of 1.14eV at room temperature.

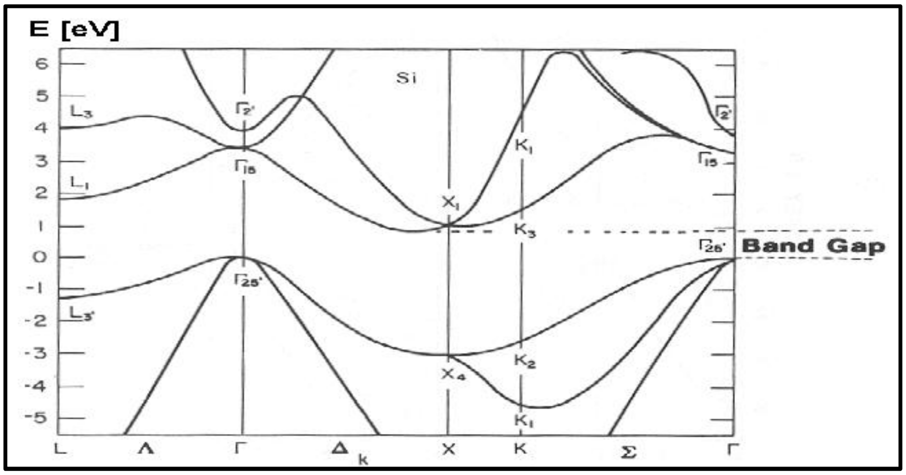

Fig. 2.2: Band gap diagram of Silicon

2.2 Quantum Confinement Effect

Reduced dimensionality and size of silicon gives advantageous properties over bulk silicon. This is caused due to quantum confinement effect occurring at nano region. Quantum confinement effect is essentially due to changes at atomic structure as a result of direct influence of ultra-small length scale on the energy band structure. The length scale corresponds to quantum confinement ranges from 1 to 25 nm for typical semiconductors of group IV, III-V, II-VI. As a result of these geometrical constraints, electrons feel the presence of particle boundaries and respond to the changes in particle size by adjusting their energy levels[32]. Quantum confinement becomes more important when the semiconductor nanostructure approaches to equal or below the bulk semiconductor's Bohr exciton radius which makes materials exhibiting size dependent properties[33].

Bohr exciton radius of a material is given by

$$a_b = \varepsilon \frac{m}{m^*} a_0 \tag{2.1}$$

where ε is the dielectric constant of material, m* is the effective mass of electron, m is the rest mass of electron, a_0 is the bohr radius of hydrogen atom. Quantum confinement effect leads to collapse of continuous energy band gap of bulk materials into discrete i.e. atomic like energy levels in NSs.

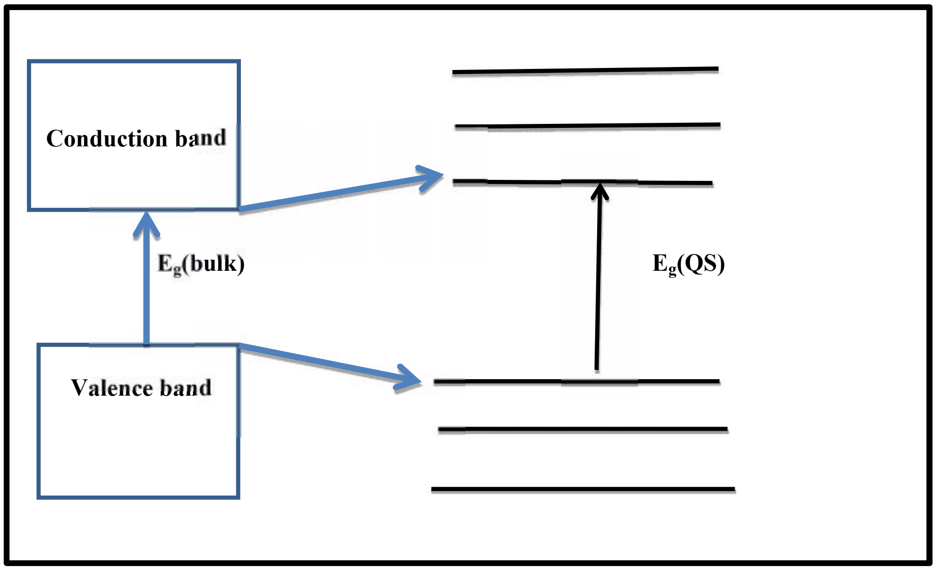

Fig. 2.3: A schematic of the discrete energy levels of a semiconductor

A quantum confined structure is one in which motion of carriers is confined in one or more directions due to potential barriers. Based on confinement directions, structures are classified in three categories in Table 1.

Table 2.1 Classification of quantum confined structures.

Structure	**Number of Confined Directions**	**Degree of freedom**
Bulk	0	3
Quantum well	1	2
Quantum wire	2	1
Quantum dot	3	0

2.3 Decoration effect on SiNWs

Decorated SiNWs arrays yielded significant enhancement in solar energy conversion efficiency, demonstrating them to be a promising hybrid system for efficient solar energy conversion[34]. More recently, decorated AuNPs on SiNWs surface, and further demonstrated that the prepared AuNPs-decorated SiNWs could produce sufficient heat under near-infrared (NIR) irradiation. Here it is important to note that SiNWs had absorption at NIR region and convert NIR light into heat, whereas AuNPs coated on surface of SiNWs significantly improve the conversion of light to heat. As a result, such SiNWs-based nanohybrids, served as noble hyperthermia nanoagents[35].

2.3.1 Role of metal decoration[36]: LSPR (Localized surface plasmon resonance)

It is now known that the intrinsic properties of MNPs are mainly governed by their size, shape, composition, crystallinity and structure. In principle, one could control any one of these parameters to fine-tune the properties of these NPs. Characteristically, noble MNPs exhibit a strong absorption band in the visible region, and this is indeed a small particle effect[37–39]. The physical origin of the light absorption by MNPs is the coherent oscillation of the conduction band electrons against the positive nucleus induced by the interacting electromagnetic field. The electromagnetic surface waves can propagate along the interface between conducting materials and a dielectric over a broad range of frequencies, ranging from dc and radio frequencies up to the visible. The oscillation modes comprise an electromagnetic field coupled to the oscillations of conduction electrons and are called surface plasmons. These are characterized by strong field enhancement at the interface, while the electric field vector decays exponentially away from the surface[40,41] . An absorption band results when the incident photon frequency resonant with the collective oscillation of the conduction band electrons and is known as the surface plasmon resonance (SPR). And the frequency at which the MNPs oscillate is called surface plasmon frequency which is given by

$$\omega_{sp} = \frac{\omega_p}{\sqrt{1+\epsilon_m}} \qquad (2.2)$$

where ω_p is bulk plasmon frequency given by

$$\omega_p = \sqrt{\frac{ne^2}{\epsilon_0 m^*}} \qquad (2.3)$$

The oscillation frequency is critically determined by factors: the density of electrons (n), the effective electron mass (m*), dielectric constant, shape, and the size of the charge distribution. For many metals such as, Pb, In, Hg, Sn, and Cd, the plasma frequency lies in the UV part of the spectrum and such NPs do not display strong color effects. The coinage metals like Cu, Ag, Au, Pt etc. are exceptional. First, they are nobler and form air-stable colloids. Second, due to d-d band transitions, the plasma frequency lies in the visible part of the spectrum. Third, at the plasmon frequency the imaginary part of the dielectric constant is very small, and this is why the near-field effect is so high that makes the plasmon excitation very interesting. Hence, surface plasmon experiments are most commonly carried out with Cu, Ag, and Au. The resonance frequency of SPR is strongly dependent upon the size, shape, interparticle interactions, dielectric properties, and local environment of the nanoparticle.

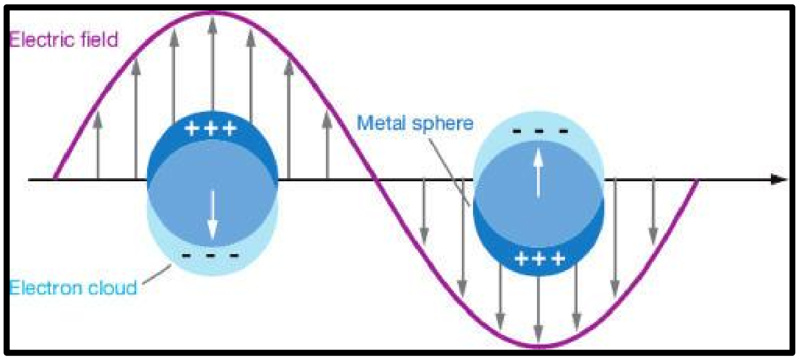

Fig. 2.4: localized surface plasmon resonance[42]

Confinement and quantization of conduction electrons within a small volume enhance the optical and electronic conductance properties of materials composed of nanocrystals. When the dimension of the NPs becomes smaller than the wavelength of the exciting light, energy can be confined in the small spatial regions through the local excitation of surface plasmon resonances. The enhanced fields in these regions are used in a wide range of applications including optical energy transport, chemical and biological sensors, surface-enhanced Raman scattering (SERS) and nanoscale optical devices[43–46]. It was also predicted that the electromagnetic field enhancement may be very large when two resonant particles are brought close to each other and most of the energy is located between the particles.

2.4 Photoluminescence

Photoluminescence is light emission process from any matter after the absorption of a photon (electromagnetic radiation). It is one of the many forms of luminescence in which relaxation process occurs by re-radiating the other photons.

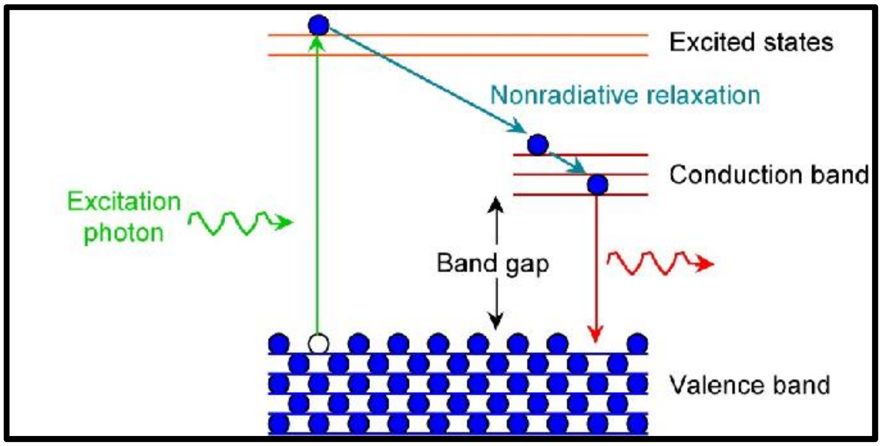

Fig. 2.5: Absorption and emission process in inter band transition

Time period between absorption and emission may vary from femtoseconds for free carrier in inorganic semiconductors which is called fluorescence; to delay of minutes to hours in molecular systems called phosphorence. All the emission or recombination processes are not radiative in nature depending upon the type of band gap of material i.e direct band gap and indirect band gap.

Band gap is the minimum energy difference between top of conduction band and bottom of valence band. When a photon is absorbed an electron-hole pair is generated and electron is excited to high energy states in conduction band.

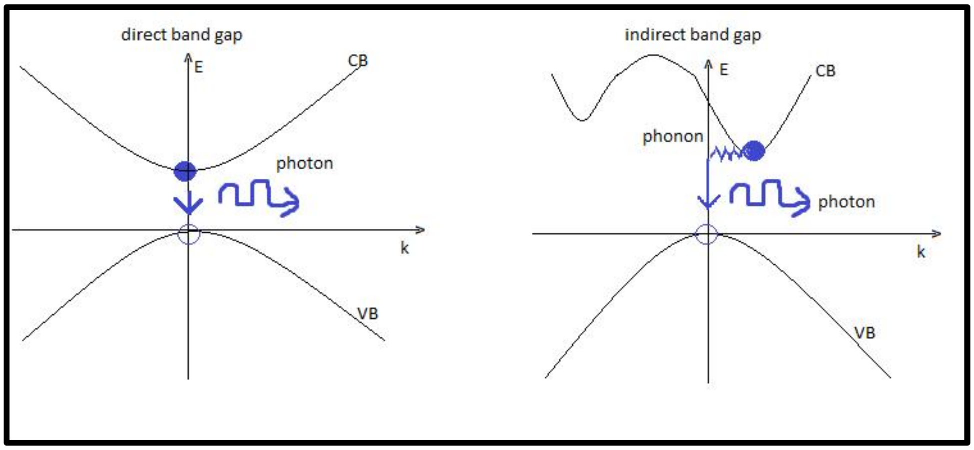

Fig. 2.6: The E-k diagram of direct (left) and indirect (right) bandgap semiconductors

During photon absorption in semiconductors, we must conserve both energy and momentum. In direct band gap semiconductors, the top of conduction band and minimum of valence band occur at same (k) momentum value and gives radiative recombination. Both photon absorption and emission (i.e electron- hole recombination) conserve the momentum without assistance of phonons, since the momentum of absorbed or emitted photon (which is in the order of $2\pi/\lambda \sim 10^5$ cm^{-1}) is negligible compared to momentum of electron (which is related to the size of the Brillouin zone $\pi/a \sim 10^8$ cm^{-1}). Therefore we represent vertical arrows in absorption and emission of photons in E-k diagrams of direct band gap[47,48].

While in indirect band gap semiconductors, conduction band minima and valence band maxima occur at different k values. As a result, to conserve momentum, the photon absorption process must involve emission of phonon leading to non-radiative recombination. Since the energy of phonon (~0.01eV) is much smaller than the energy of the PL photon, so the peak energy of the PL also roughly reflects its band gap.

For particles in nanometer region, we would expect substantial change in PL peak energy and efficiency (ratio of absorbed photons to emitted photons) due to quantum confinement effect. The conversion of indirect bandgap material to direct band gap material can also be easily achieved by quantum confinement effect. This could be understood in terms of Heisenberg Uncertainity principle. If Δx and Δk are the uncertainties in the position and wave-vector respectively, uncertainty principle invokes $\Delta k.\Delta x \sim 1$. In bulk materials, Δx is infinity because of its crystalline nature. Thus only transitions with $\Delta k = 0$ is allowed by the uncertainty principle. In a NS of size *'L'*, the uncertainty in position is *'L'* which brings an uncertainty of $1/L$ in the momentum (i.e. $\Delta k \sim 1/L$). All the transitions are allowed when Δk lies in the range of $1/L$. Therefore, optical recombination is possible in appropriately low dimensional materials. As a consequence, it can be said that the band gap is effectively a direct type in nature for optical transitions to take place. In low dimensional materials, no phonon is involved in the intermediate process. This observation is very important in developing optical devices using materials which show an indirect band gap in the bulk form.

2.5 Diffuse reflectance spectroscopy (DRS)

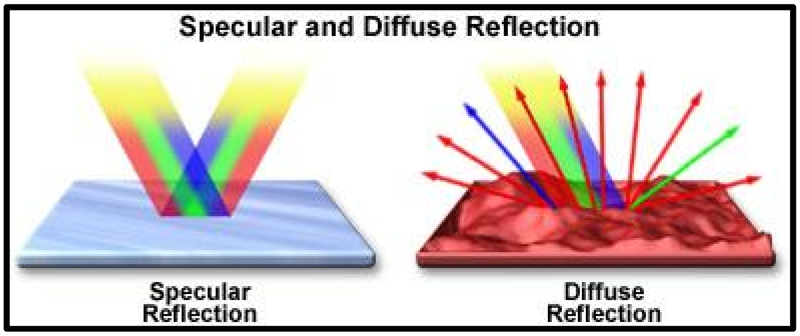

Fig. 2.7: Specular and diffuse reflection on smooth and rough surface respectively[49]

Depending upon the topology of the surface of the material there are two types of reflection specular reflection and diffuse reflection. When incident light reflected symmetrically with respect to the normal line, it is called specular reflection. Reflection on smooth bodies, calm water etc. leads to specular reflection. When incident light scattered in different directions after reflection, it gives diffuse reflection e.g. on rough surfaces, porous surfaces, roads etc.

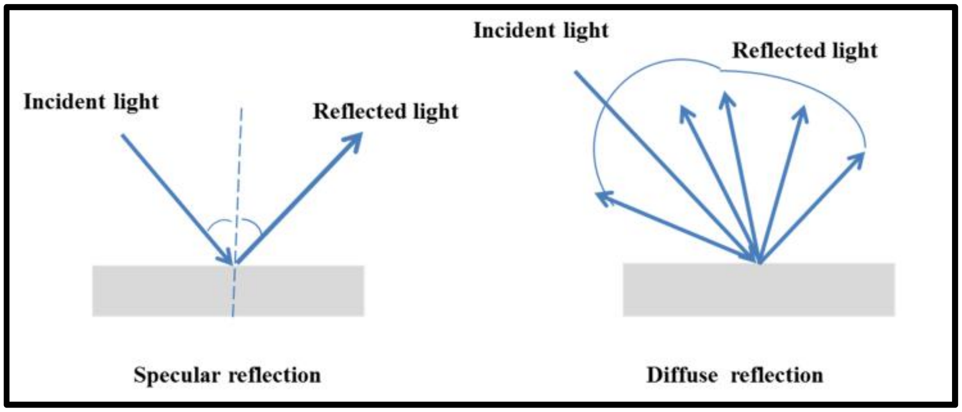

Fig. 2.8: Schematic diagram of specular and diffuse reflection

For each type of reflection, individual ray follows law of reflection. In diffuse reflection, the roughness of material means there are different normal lines for different rays. This result in a bundle of light incident on surface and get diffused on reflection in many directions.

2.5.1 How diffuse reflection helps?

Determination of band gap is important to know the basic physics of materials. Moreover the quantum confined structures results in widening of band gap that has to be estimated to confirm the NSs formation.

When light shines on rough sample it reflects in all directions due to variation in surface. The remainder of light is refracted in the sample where it is scattered due to internal reflections. Some of the scattered light is emitted back into the air. The diffused light reflected back become weaker if absorption occurs in the sample. This implies that the out coming diffused light depends upon the light absorbed in the sample if transmission is controlled somehow.

2.5.2 Band gap estimation from diffuse reflectance using Kubelka-Munk function

Kubelka-Munk model allows the band gap estimation of unsupported materials like powder or rough films. Eventually the band gap estimation of powder and rough film is not possible by typical UV spectroscopy. Basically Kubelka-Munk function is directly proportional to the absorption coefficient of the material[50]. DRS spectra of the samples are converted to equivalent absorption using Kubelka-Munk function $F(R_\infty)$ for infinitely thick samples which is given by[51–53]

$$F(R_\infty) = \frac{K}{s} = \frac{(1-R_\infty)^2}{2R_\infty} \qquad (2.4)$$

Where, $R_\infty = R_{sample}/R_{standard}$. R_{sample} is the diffuse reflectance of the sample and $R_{standard}$ is diffuse reflectance of the standard sample ($BaSO_4$ in the present case). K and S are the Kubelka–Munk absorption and scattering functions, respectively. After getting Kubelka-Munk absorption, the band gap estimation can be done by well know method using Tauc plot[54–56] in the following manner:

The following relational expression proposed by Tauc, Davis, and Mott is used.

$$(h\nu\alpha)^{1/n} = A(h\nu - E_g) \qquad (2.5)$$

Where, h is Planck's constant, ν is frequency of incident photon, α is absorption coefficient, E_g is band gap and A is proportionality constant.

The value of the exponent n denotes the nature of the sample transition.

For direct allowed transition···········n = 1/2

For direct forbidden transition·········n = 3/2

For indirect allowed transition·········n = 2

For indirect forbidden transition·······n = 3

Since $F(R_\infty)$ is proportional to the absorption coefficient. Therefore α in the Tauc equation is substituted with $F(R_\infty)$. Thus, the modified expression becomes:

$$[h\nu\, F(R_\infty)]^{1/n} = A(h\nu - E_g) \qquad (2.6)$$

Now using the Kubelka-Munk function, the $[h\nu\, F(R_\infty)]^{1/n}$ was plotted against the hν. The curve that plots the value of hν on the horizontal axis and $[h\nu\, F(R_\infty)]^{1/n}$ on vertical axis is drawn. Further a line is drawn tangent to the point of inflection on the curve and the hν value at the point of intersection of the tangent line and the horizontal axis provides band gap E_g value.

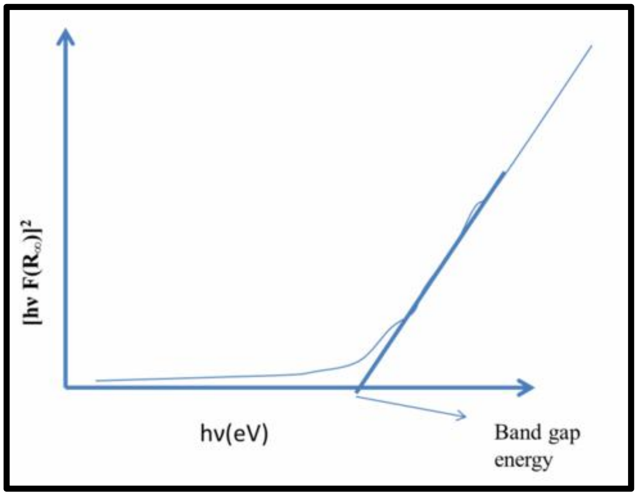

Fig. 2.9: Schematic diagram showing the band gap determined from Kubelka Munk function

Chapter 3

Experimental details

Instruments used for material characterization:

3.1. Field emission scanning electron microscope (FESEM)

Morphological study of specimen can be done very precisely by FESEM. In FESEM the electrons interact with the atoms that make up the sample producing signals containing information about sample's surface, topography, morphology, composition and other properties.

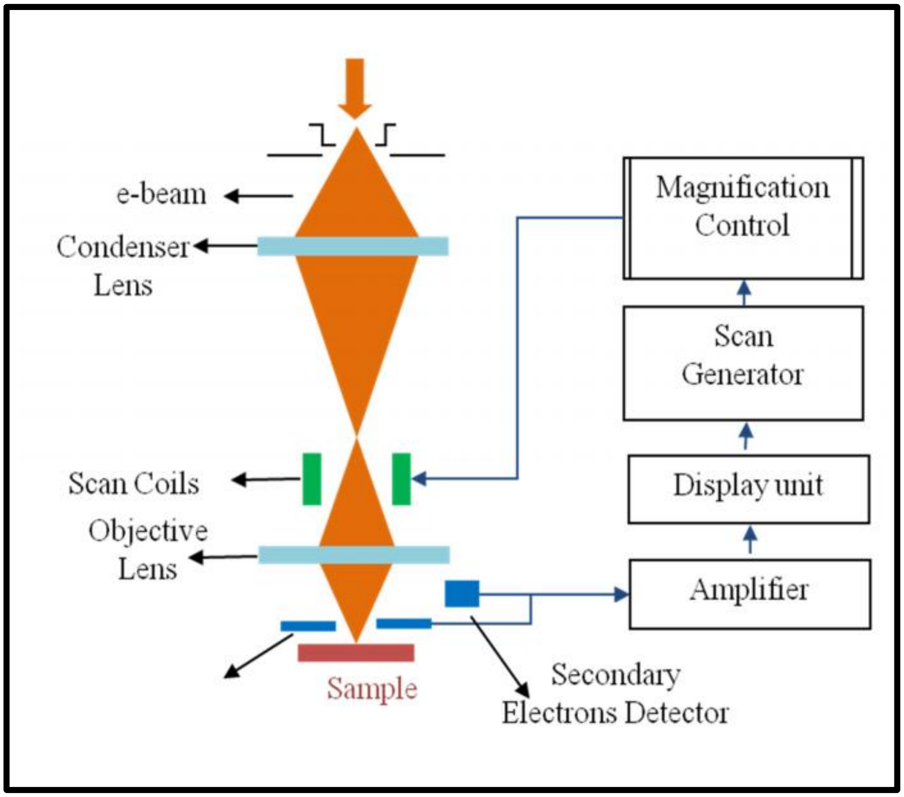

Fig. 3.1: Schematic diagram of FESEM

3.1.1 Signals generated

This interaction leads to emission of secondary electrons (SEs), backscattered electrons (BSEs), auger electrons, X-rays, etc. In case of FESEM, the interaction products most frequently used for the generation of images are (i) SEs and (ii) BSEs.

(a) Secondary electrons

When the incident electron beam enters the specimen, secondary electrons are produced from the emission of the valence electrons of the constituent atoms in the specimen. Since the energy of secondary electrons is very small generally less than 50 eV, SEs are extremely abundant and the SE yield (the number emitted per primary electron) is dependent on the accelerating voltage.

(b) Backscattered electrons

All electrons having energy higher than 50 eV are BSE and are generated by elastic scattering and BSE yield depends on atomic number Z, so information from a relatively deep region is contained in the back scattered electrons. The back scattered electrons are sensitive to the composition of the specimen. This feature can be used to observe the topography of the surface.

(c) Generation of X-Rays

When electrons in the inner shells are emitted X-rays whose energies correspond to the energy difference between the outer and inner shell electrons are generated.

(i)Energy dispersive X-ray spectroscopy (EDS)

Backscattered electrons shows compositional contrast result from different atomic number element and EDS allows one to identify those particular elements and their relative proportions. EDS is used to analyse characteristic X-ray spectra by measuring the energies of the X-rays. When the X-rays emitted from the specimen enter the semiconductor detector, electron-hole pairs are generated whose quantities correspond to the X-ray energy. EDS software associates the energy of X rays with the element and maps the previously defined elements over the scanned area. The advantage of the EDS is that the X-rays from a wide range of elements are analysed simultaneously.

(d) Imaging in SEM

The interaction of beam with sample does not occur at a point but throughout the volume, this size of volume depends on beam energy and shape of interaction volume on atomic number. High Z elements give elastic scattering i.e. more number of BSE.

3.1.2 Construction of instrument

The SEM requires an electron probe, a specimen stage to place the specimen, a secondary-electron detector to collect secondary electrons, an image display unit, and an operation system to perform various operations.

(a) Electron source

The illumination system of FESEM consists of an electron source, which is maintained at a negative potential. The emitted electron beam, which typically has an energy ranging from a few hundred eV to 30 Kev, is passed through a magnetic lens system.

(b) Condenser lens and objective lens

Placing a lens below the electron gun enables you to adjust the diameter of the electron beam.

Two-stage lenses are located below the electron gun. The objective lens is a very important that determines the final diameter of the electron probe up to 5 to 10 nm.

(c) Detector

A scintillator is coated on the tip of the detector and a high voltage of about 10 KeV is applied to it. The secondary electrons hit the scintillator and generate the light.

Two secondary electron detectors present in SEM are: In-lens (TTL) detector and Lower (ET) detector. These detectors can be used separately or combined.

Measurements show that lower detector sees a signal which is typically 40% SE3, 45% SE2, about 15% SE1. The in lens detector located above the objective lens and sees a signal mix which is about 75% SE2 and 25% SE1. The in lens detector therefore contains a much lower BS component in its signal output and so gives higher contrast images.

This light is directed to a photo-multiplier tube (PMT) and amplified, then transferred to the display unit. Since the scanning on the display unit is synchronized with the electron-probe scan, brightness variation, which depends on the number of the secondary electrons thus forming a SEM image. A cathode-ray tube (CRT) or liquid-crystal display (LCD) used as a display unit.

In this work FESEM images were recorded using Supra T M 55; Carl Zeiss.

3.2 Photoluminescence spectrometer

Photoluminescence spectroscopy is a contact-less, versatile, non-destructive method of probing the electronic structure of a material. Typically, a laser beam impinges a sample, where it is absorbed.

The excess energy brought to the material can be dissipated through the emission of light.

The basic equipment setup needed to perform conventional photoluminescence consists of two main parts:

(1) A light source to provide above or below-band-gap excitation; and

(2) A detection system to collect and analyze the photons which are emitted from the sample.

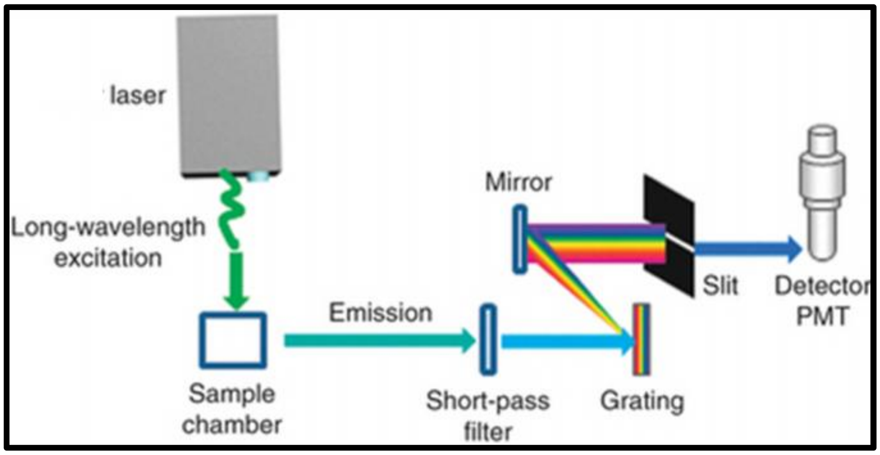

Fig. 3.2: Schematic of experimental set up for PL

3.1.1 Instrument construction

a) Excitation source

Helium Cadmium (He-Cd) laser has been used as a source for violet ultraviolet (325 nm) output. Because of their excellent beam quality, He-Cd lasers have been used extensively for diffraction grating fabrication, spectroscopy, non-destructive testing, and microlithography etc. The lasing element in He-Cd lasers is cadmium. At room temperature, cadmium is a metal. For lasing to occur, the metal must be evaporated from a reservoir, and then the vapor must be distributed uniformly down the laser bore. The distribution is accomplished through a process called electrophoresis.

The construction of He-Cd lasers is far more complex than that of other helium based lasers. The laser tube contains a reservoir for cadmium and a heater to vaporize the metal. As a result, a heated filament cathode is often used in place of the cylindrical tube that comprises a He-Ne laser. Additionally, the laser itself needs to sustain a higher level of internal pressurization allowing the vaporized cadmium to remain in the tube. The lifetime of a specific helium cadmium laser is dictated by the amount of cadmium in the reservoir. Once the cadmium supply is exhausted, the tube must be replaced.

b) Luminescence collection and detection equipment

It consists a pair of lenses, mirror, filter, monochromators, photomultiplier tube (PMT), and computer (PC). The simplest fixed filters are used to isolate both the excited and emitted wavelengths. To isolate one particular wavelength from a source emitting a pair of cut-off filters is required. These may be either glass filters or solutions in cuvettes.

A further refinement would be to use monochromators to select the emission wavelengths. Most instruments of this type employ diffraction grating monochromators for this purpose. The light is spatially split up by a dispersion element such as a prism or a grating. The emitted light enters through a slit shaped entrance aperture of variable width and shines on to a collimation mirror. The mirror is used to parallelise the light, so that the grating is evenly illuminated. As a reflection grating is used, light of different wavelengths is reflected in different directions. Another diffractive mirror focuses the light onto the detector where different wavelengths are detected at different positions on the detector. Thus signal was spectrally resolved with monochromators.

Fluorescence instruments use photomultiplier tubes as detectors. The material from which the photocathode is made determines the spectral range of the photomultiplier. The spectral response of all photomultipliers varies with wavelength, but it is sometimes necessary to determine the actual intensity of the incident radiation. A suitable quantum counter can be made solution which has the property of emitting the same number of quanta of light as it absorbs, but over a very wide wavelength range. Thus, by measuring the output of the quantum counter at one wavelength, the number of incident quanta over a wide wavelength range can be measured. The output from the detector is amplified and displayed on a readout device which may be a meter or digital display.

3.3 Diffuse reflectance spectrometer

A diffuse reflectance has been measured by an attachment to an UV-Vis spectrometer. Here an integrating sphere detector (Fig. 3.3(b)) is attached to Carry 60 (Agilent) UV-Vis instrument (Fig. 3.3(a))

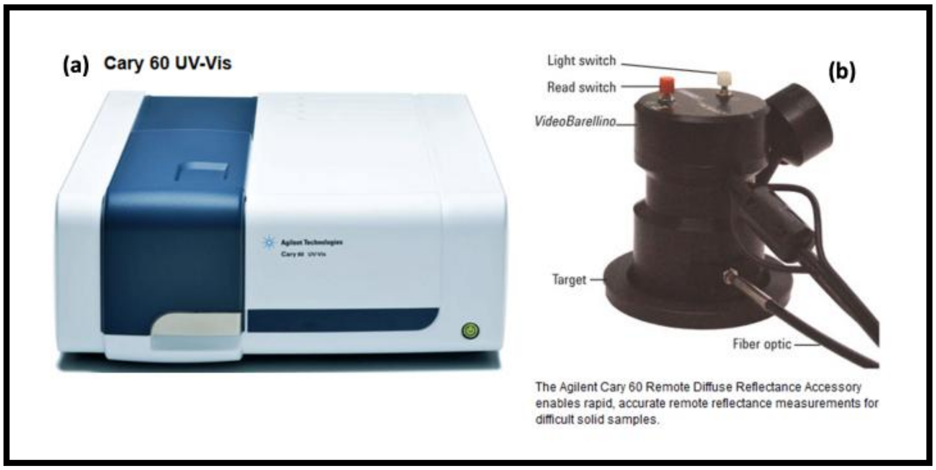

The Agilent Cary 60 Remote Diffuse Reflectance Accessory enables rapid, accurate remote reflectance measurements for difficult solid samples.

Fig. 3.3: Experimental set up for diffuse reflectance measurement (a) Carry 60 UV-Vis spectrometer, (b) an integrating sphere attachment to detect diffuse reflectance

In Carry 60 white lamp sources (xenon lamp) is used and grating is used to select monochromatic wavelength. Here in this set up the initial beam is splitted in two parts, one is taken as reference beam and second goes on the sample. Finally the output is compared to the reference beam and data has been collected. Since output photons comes through scattering from the samples so there is an integrating sphere detector. With integrating sphere, measurement is performed by placing the sample in front of incident light and concentrating the light reflected from the sample on detector using a sphere coated with barium sulfate inside. The obtained value becomes reflectance with respect to reflectance of standard white paper which is 100%.

3.4 Sample preparation

3.4.1 Method used for preparation

Metal induced etching (MIE) method is adopted for fabricating SiNWs. Amongst various methods used for fabrication of Psi/SiNs, MIE is one of the simplest and cheapest methods for synthesis of semiconductor NSs. The schematic of formation SiNWs has been shown in Fig. 3.4

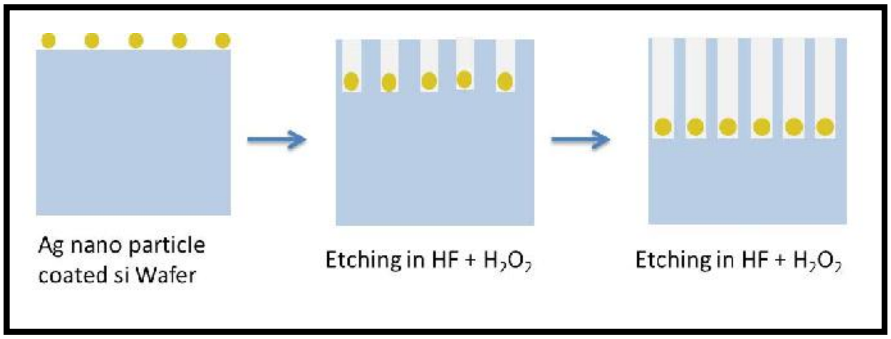

Fig. 3.4: Schematic diagram of the formation of SiNWs

The steps involved in sample preparation are discussed below.

(i) Substrate cutting and cleaning

Silicon wafers of required dimensions were cut using a diamond tip glass cutter. Cleaning of substrates is critical for sample fabrication by MIE; these were cleaned to remove inorganic impurities. Substrates were subsequently cleaned in acetone and iso-propanol solutions for 10 min each.

(ii) Surface treatment

Substrates were further washed with 5% HF solution to remove the thin oxide layer that is formed on the surface of silicon wafer due to exposure to air and then with distilled water to remove excessive fluoride ions.

(iii) Metal deposition

These wafers were then dipped in solution containing 4.8M HF and 5mM $AgNO_3$ for required deposition time to deposit AgNPs and then rinsed with distilled water to remove extra silver ions. This step is crucial to determine the diameter of SiNWs.

(iv) Etching process

The AgNPs deposited samples were then kept for etching in an etching solution containing 4.6M HF and 0.5M H_2O_2 according to desire. Etching time decides the length of the SiNWs. This step is also known as porosification time.

(v) Removal of Ag particles after porosification

Etched wafers were transferred to HNO_3 to remove AgNPs after the etching process. Then the samples were dipped into HF solution to remove oxide layer induced by HNO_3 used in above step.

(vi) Decoration of MNPs

Decoration of SiNWs is done by sputtering method. The model Q150R ES use easy-change, 57 mm diameter, disc-style targets which are designed to sputter non-oxidizing (noble) metals. The Q150R ES are fitted as standard with a gold (Au) sputter target. Only Au and Pt are used to decorate SiNWs in this project.

Table 3.1: List of samples prepared

Sample	Deposition time (sec)	Etching time (minute)	Decoration
S	60	60	None
S1	60	30	None
S2	60	45	None
S3	60	60	None
DS1	60	60	Gold (Au)
DS2	60	60	Platinum (Pt)

Chapter 4

Result and Discussion

4.1 Mechanism of metal induced etching

MIE mechanism is very simple and popular method to fabricate semiconductor NSs [1–7] . As already mentioned in chapter 3 the MIE involves mainly two steps, (i) deposition of MNPs on a clean Si wafer and (ii) etching of this metal deposited wafer in an etching solution consisting of HF and H_2O_2. In the present study, AgNPs have been used, which is deposited on Si wafer by dipping a clean Si wafer into a solution of $AgNO_3$ and HF. Ag^+ ions, available in this solution, when come in contact with Si surface, accept one electron from the Si and get neutralized as AgNPs. The transfer of electron from Si to Ag^+ is favorable because the redox energy for the pair Ag^+/Ag (0.79 V) is higher than the valence band energy of Si (0.62 V) [8]. This transfer of electron from Si to Ag^+ results the injection of hole (h^+) (creation of positive site in Si) in the Si. The injection of hole inside the Si is necessary to start the porosification [3, 9–11] using HF acid. These AgNPs deposited Si wafers are put into the etching solution of HF and H_2O_2 where the positive sites of Si, created in the previous step, gets attacked by fluoride ion (F^-). This forms H_2SiF_6 before getting dissolved in HF solution and creates a pit on the Si surface.

Further, transfer of another electron from Ag to H_2O_2 takes place which results in reduction of H_2O_2 and creation of Ag^+ to start next cycle of etching by providing continuous supply of Ag^+ and thus of h^+. For this process, transfer of electron is favorable because the redox energy for the pair H_2O_2/H_2O (1.78 V) is higher than the redox energy for the pair Ag^+/Ag (0.79 V) [8]. In this way the AgNPs penetrate deeper into the wafer as porosification proceeds. The etching time (continuation of cycle) decides the depth of pits in the Si. A schematic to show the above-mentioned processes involved in MIE has been shown in Fig. 4.1 which is dictated step by step in details as follows: (1). Ag^+ ion available in solution, sits on Si wafer takes one electron from Si wafer and create positive site in Si. (2) F^- ions available in solution of HF and H_2O_2, attacks on the positive sites of Si. (3) As a result of reaction between F^-ion and Si at the positive sites, H_2SiF_6 formed. In this way Si atoms get out from Si wafer and result pit in Si wafer.

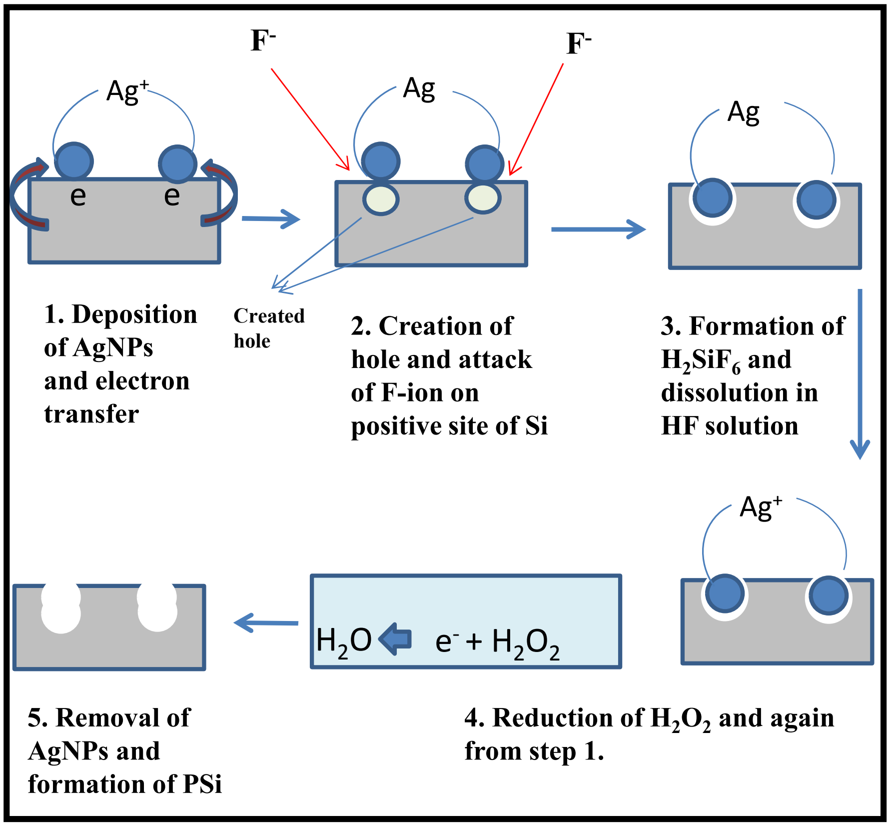

Fig. 4.1: The schematic diagram of formation mechanism of Si NSs during MIE

(4) To repeat the above process (step 1 to step 3), H_2O_2 takes one electron from Ag to form Ag^+. This process repeated again and again which decides the depth of pits and can be controlled by the etching time (time of living of AgNPs deposited Si wafer in etching solution). (5) Finally after the particular etching time, the AgNPs are removed by the dipping that wafers in HNO_3 and obtained SiNWs on Si wafer.

The chemical reactions involved in fabrication of Si NSs using porosification by MIE are:

$$Ag^+ + e^- \rightarrow Ag, \qquad \text{Creation of hole (1)}$$

$$Si + 4h^+ + 6HF \rightarrow H_2SiF_6 + 4H^+, \qquad \text{Silicon dissolution (2)}$$

$$H_2O_2 + 2Ag \rightarrow 2H_2O + 2Ag^+ + 2e^-, \qquad \text{Repeat etching cycle (3)}$$

4.2 Surface morphologies of Si NSs

Surface morphologies of different samples, containing Si NSs, fabricated by MIE method have been studied using SEM. A systematic SEM image study helps in understanding the process involved in the MIE.

4.2.1 Formation of Si NSs by MIE

MIE protocol has been adopted as it is to fabricate Si NSs. All the steps involved in MIE (discussed in chapter 3) are followed. Therefore starting has been done by the cleaning the Si wafer surface. Figure 4.2a reveals that Si surface is clean and can be used for further analysis. The cleaned Si wafer is dipped into the solution of $AgNO_3$, and HF for the deposition of AgNPs for 1 min at room temperature. Ag^+ available in the solution of $AgNO_3$ and HF sit on the clean Si wafer and deposited in the form of AgNPs on Si wafer. Surface morphology of AgNPs deposited Si wafer is shown in Fig. 4.2b which reveals that the uniform AgNPs has been deposited on the Si surface.

Further AgNPs deposited Si wafer is dipped into the etching solution of HF and H_2O_2 for 60 min then rinsed with distilled water and put into HNO_3 solution for removing of Ag from the sample (sample S table 3.1). Now again the surface morphology of etched sample S has been investigated using SEM.

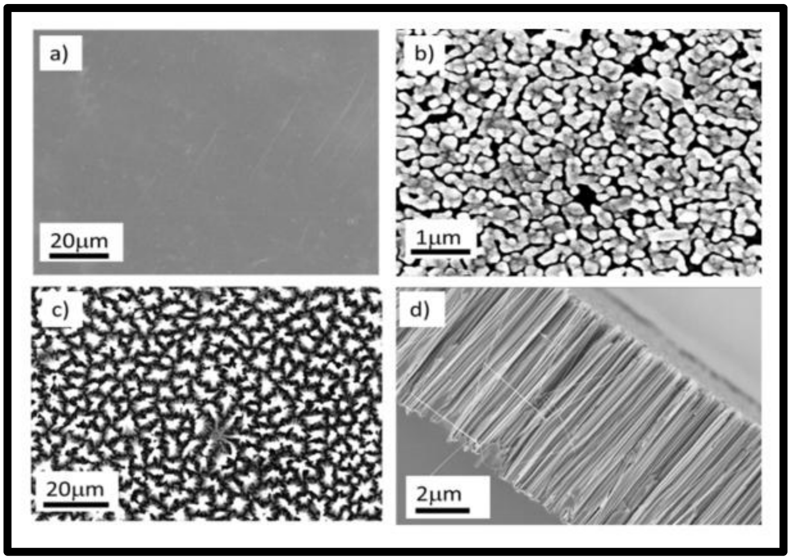

Fig. 4.2: Surface morphology of (a) clean surface of Si (b) AgNPs deposited Si wafer, (c) sample S (d) cross-sectional surface morphology of sample S.

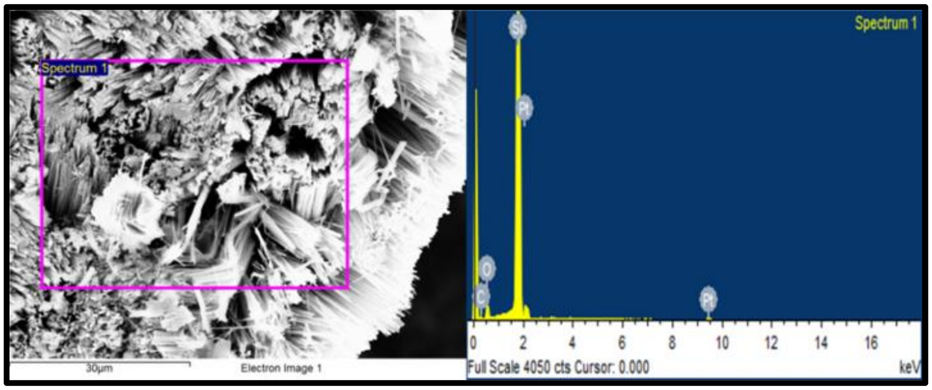

Fig. 4.3: SEM image (left) and EDX analysis (right) of Pt D- SiNWs

Figure 4.2c shows the surface morphology of etched sample and it can be seen that the uniform pores are fabricated on the Si surface. This figure also suggests that there may be wire like structures available in the samples. To confirm the wire like structures, cross-sectional SEM has also been done. The cross-sectional SEM results of etched sample shown in Fig 4.2d. Figure 4.2d reveals that dense SiNWs have been successfully fabricated by using MIE. The length of the wire is estimated by SEM result and found to be approximately 80 μm. After successful fabrication of SiNWs, SiNWs are decorated with Au and Pt as discussed in chapter 3. SEM image and EDS analysis of Pt D-SiNWs are shown in figure 4.3.

4.3 Optical properties of SiNWs and D- SiNWs

4.3.1 Photoluminescence

PL spectroscopy is very important tool for the characterization of nanomaterials [1–3] because most of the nanomaterials exhibit PL (due to quantum confinement effect). A room temperature PL in Si itself proves that Si NSs are in nano regime because Si (having 1.1 eV indirect band gap) in the bulk form does not exhibit room temperature PL in visible region. Therefore PL spectroscopy has been carried out to investigate the PL properties of Si. The excitation energy of photon to carry out PL, used in thesis work is 3.81 eV (He-Cd laser).

Figure 4.4 shows the PL spectra from SiNWs sample and inset displays the photograph of luminescence coming from SiNWs samples (recorded by camera). Visible room temperature PL (RTPL) from SiNWs confirms that nanostructures formed in samples are in nano regime. Figure 4.4 shows the PL peak around 640 nm and a broad hump from 390 nm to 480 nm. This broad hump can be assigned to the presence of SiOx present in the samples[4]. However it is also interesting that most of the times, RTPL from SiNWs fabricated by wet chemical etching exhibit red emission only irrespective of etching time and other fabrication parameters (data shown in appendix B, Fig. B1)

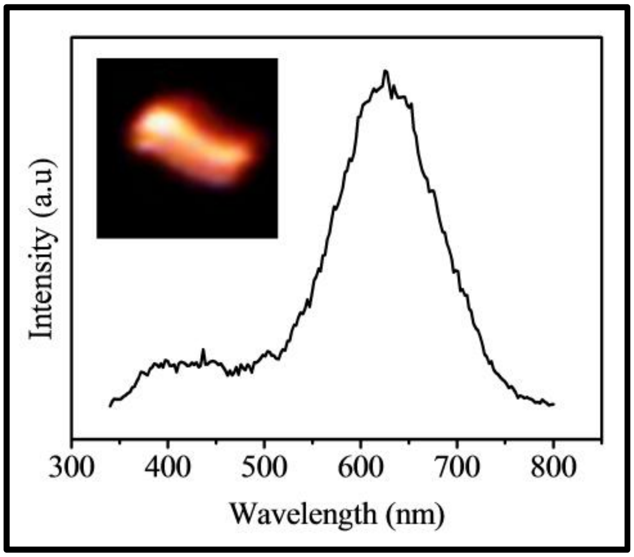

Fig. 4.4: Room temperature Photoluminescence spectrum from SiNWs. Inset shows a photograph of luminescence from SiNWs (sample S) under UV excitation

The reason behind the red emission can be understood by Wolkin's model[5] which suggests that Si nanocrystallite is passivated by oxygen, a stabilized electronic state (or even a trapped exciton) may be formed on the Si=O covalent bond. The electron state is a p state which localized on Si atom and the hole of p state localized on the oxygen atom [25]. Therefore PL energies are fixed even if the band gaps of SiNWs are changing as the size of SiNWs goes decreasing.

To investigate the effect of MNPs decoration on the RTPL of SiNWs, PL spectroscopy again performed for D-SiNWs. Figure 4.5 shows the PL spectra from SiNWs decorated by gold (sample DS1) and bare SiNWs (sample S) samples. It is clear from Fig. 4.5, PL peak from D-SiNWs is broad and blue shifted as compared to SiNWs PL.

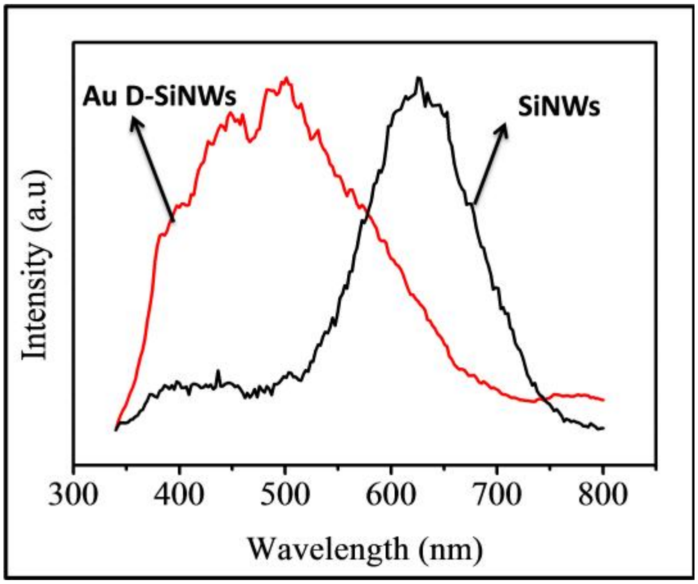

Fig. 4.5: Room temperature photoluminescence spectra from sample S and DS1.

The shift in PL can be understood by exciton-plasmon coupling[4,6–8]. The enhancement and quenching of PL intensity depends on the difference between PL energy and plasmon energy of MNPs where both the energy coincides, multi-fold PL enhancement occurs. In Fig. 4.5 PL peak observe around 510 nm which coincides with Au plasmon resonance peak hence PL enhancement occurs here. It is also clear from Fig. 4.5 that PL is quenched away from 560 nm. This quenching of PL is due to the mismatch of plasmon resonance energy and PL energy of SiNWs. Again there some PL enhancement of around the 720 nm, this is also due to energy match of localized plasmon energy of gold[9] and excitonic transition within SiNWs. This trend of PL (enhancement and quenching) establishes the coupling phenomenon between excitonic transition and plasmon resonance.

Figure 4.6 shows the PL spectrum from D-SiNWs by Pt NPs (sample DS2) also seems to be broad and blue shifted as compared to PL spectrum from bare SiNWs. This can also be understood from exciton plasmon coupling. In the other words the matching of plasmon energy gives rise to PL intensity (PL enhancement) and mismatching arise quenching in PL intensities. This would be more clear from absorption near the plasmon energy which is consistent with PL results. This will be discussed in next section.

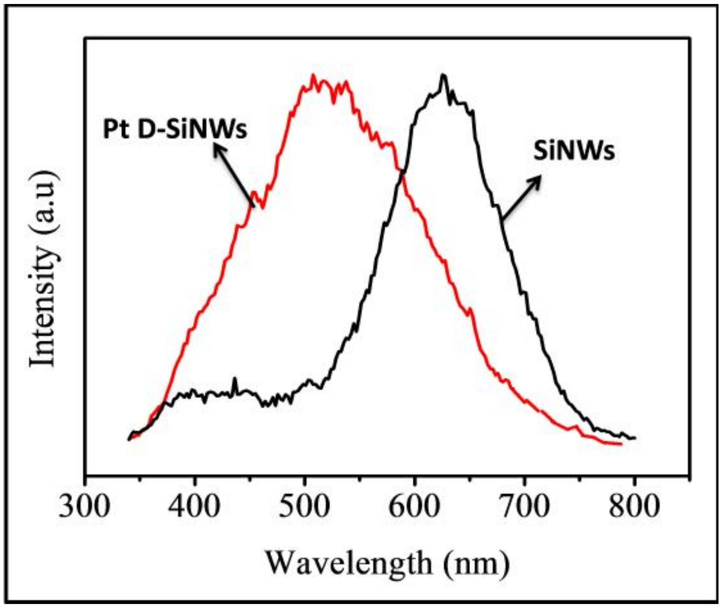

Fig. 4.6: Room temperature photoluminescence spectra from D-SiNWs by platinum and SiNWs

It is also important to mention here that it is very difficult to get match between excitonic transition energy and plasmon resonance energy which is one of the necessary condition for the PL enhancement.

4.3.2 Absorption

Qualitative and quantitative absorption of semiconductor material is very important parameter for the optoelectronic application. There were several attempts[10–13] to improve the optical absorption of Si for photovoltaic application. SiNWs have been proved a better option over porous Si due the trapping of light in SiNWs by multiple reflections. To investigate the optical absorption of SiNWs and D-SiNWs, DRS spectroscopy has been done.

Figure 4.7 shows the Kubelka Munk absorption of SiNWs and D-SiNWs by gold MNPs. It is clear from Fig. 4.7 that the absorption of sample DS1 are higher (in the visible range) than bare SiNWs. Here a small hump around 510 nm is observed which corresponds to plasmon energy peak of gold MNPs. It is consistent with PL result where the enhancement in PL intensity near to this plasmon energy found. Apart from this, decoration of SiNWs may enhance the optical absorption which may be better candidate for solar cell application.

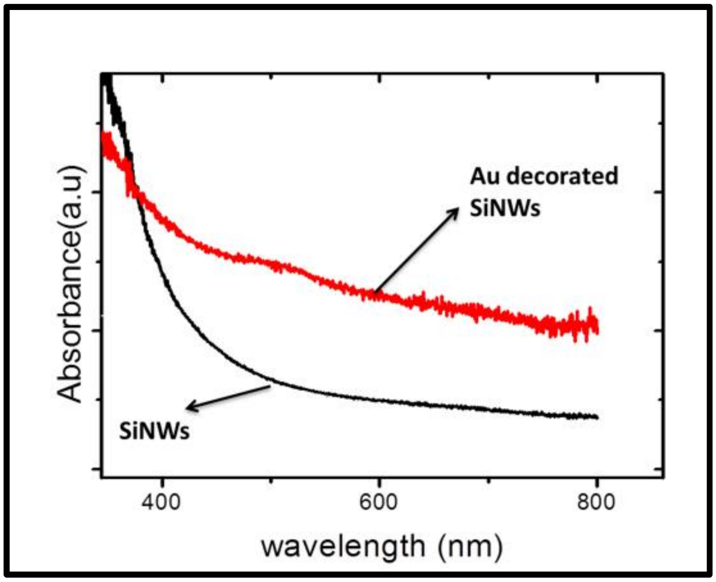

Fig. 4.7 Optical absorption spectra of SiNWs (sample S) and D-SiNWs (sample DS1)

Again the absorption of D-SiNWs by Pt MNPs (sample DS2) has studied. Figure 4.8 shows absorption spectra of Pt D-SiNWs and bare SiNWs.

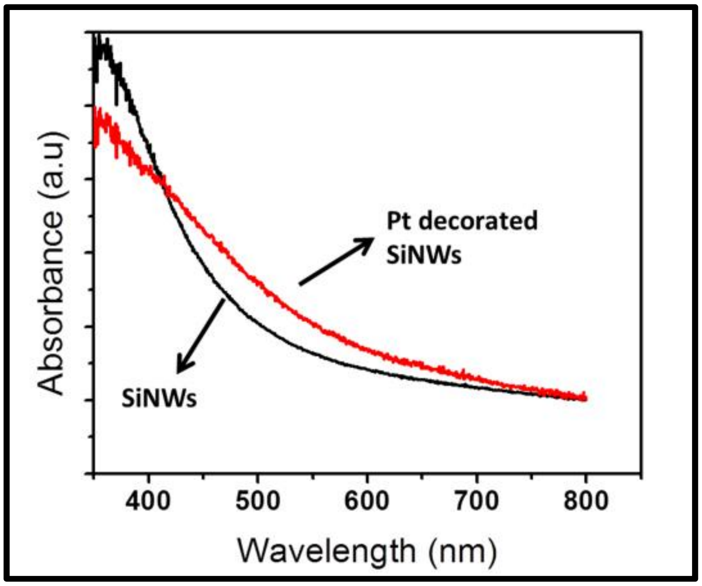

Fig. 4.8 Optical absorption spectra of sample S and sample DS2

Figure 4.8 reveals that Pt decorated SiNWs are having better absorption as compared to bare SiNWs. Here enhancement of absorption is in the range 400-600nm which is also consistent with PL results. However the enhancement of absorption is better in the case of gold decorated SiNWs than platinum decorated SiNWs.

Therefore there exists exciton-plasmon coupling in D-SiNWs. The exciton-plasmon coupling decides the enhancement or quenching of PL which also depends on the matching of plasmon resonance energy with the PL energy.

Overall the optical properties of SiNWs have been improved by decoration of SiNWs by noble metals

Chapter 5

Conclusion and Future Scope

5.1 Conclusions

The major conclusions of the research work reported in this thesis are being summarized below:

- Well aligned SiNWs can be prepared by MIE technique.
- In MIE metal nanoparticles provides sites for porosification to start and more coverage of MNPs result in thinner SiNWs/wider pores.
- Exciton plasmon coupling in decorated SiNWs has been studied which is responsible for the enhancement and the quenching of PL of SiNWs.
- There is a significant enhancement in absorption of decorated SiNWs as compared to bare SiNWs.

5.2 Future scope

There are some possible scopes to extend this work further in future as:

- Understanding of MIE can be utilized for the formation of other semiconductor NSs such as Ge NSs, GaAs NSs etc.
- These D-SiNWs systems can be utilized for the in depth study of physical phenomenon like exciton-plasmon coupling and energy transfer etc occurring at the interface of metal and semiconductor.
- The significant absorption observed in D-SiNWs may be good candidate for the solar cell application.

APPENDIX-A

Specification list of Silicon Material

Property	**Value**	**Units**
Atomic mass	28.09	amu
Atomic density	4.995×10^{14}	atoms/cm^2
Boiling point	2,878	^{o}C
Density	2.33	g/cm^3
Energy Gap	1.12	eV
Dielectric constant	11.8	
Refractive index	3.4	
Lattice constant	0.543	nm

APPENDIX-B

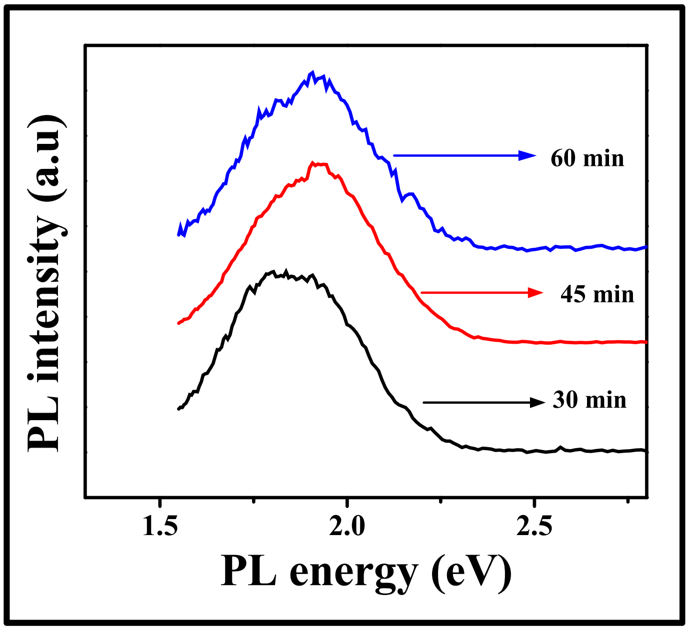

Figure (B1) : Etching time independent PL peak for sample S1, S2 and S3.

REFERENCES

[1] L. Pavesi, L. Dal Negro, C. Mazzoleni, G. Franzò, F. Priolo, Optical gain in silicon nanocrystals, Nature. 408 (2000) 440–444. doi:10.1038/35044012.

[2] Z. Ding, B.M. Quinn, S.K. Haram, L.E. Pell, B.A. Korgel, A.J. Bard, Electrochemistry and electrogenerated chemiluminescence from silicon nanocrystal quantum dots, Science. 296 (2002) 1293–1297. doi:10.1126/science.1069336.

[3] G.F. Grom, D.J. Lockwood, J.P. McCaffrey, H.J. Labbe, P.M. Fauchet, B. White, J. Diener, D. Kovalev, F. Koch, L. Tsybeskov, Ordering and self-organization in nanocrystalline silicon, Nature. 407 (2000) 358–361. doi:10.1038/35030062

[4] J.E. Allen, E.R. Hemesath, D.E. Perea, J.L. Lensch-Falk, Z.Y. Li, F. Yin, M.H. Gass, P. Wang, A.L. Bleloch, R.E. Palmer, L.J. Lauhon, High-resolution detection of Au catalyst atoms in Si nanowires, Nat. Nanotechnol. 3 (2008) 168–173. doi:10.1038/nnano.2008.5.

[5] Z. Huang, N. Geyer, P. Werner, J. de Boor, U. Gösele, Metal-Assisted Chemical Etching of Silicon: A Review, Adv. Mater. 23 (2011) 285–308. doi:10.1002/adma.201001784.

[6] A. Wolfsteller, N. Geyer, T.-K. Nguyen-Duc, P. Das Kanungo, N.D. Zakharov, M. Reiche, W. Erfurth, H. Blumtritt, S. Kalem, P. Werner, U. Gösele, Comparison of the top-down and bottom-up approach to fabricate nanowire-based silicon/germanium heterostructures, Thin

Solid Films. 518 (2010) 2555–2561. doi:10.1016/j.tsf.2009.08.021.

[7] R.H.J. Hannink, A.J. Hill, Nanostructure Control of Materials, Woodhead Publishing, 2006.

[8] M. Husain, Z.H. Khan, Advances in Nanomaterials, Springer, 2016.

[9] G. Ledoux, J. Gong, F. Huisken, Effect of passivation and aging on the photoluminescence of silicon nanocrystals, Appl. Phys. Lett. 79 (2001) 4028–4030. doi:10.1063/1.1426273.

[10] A.G. Cullis, L.T. Canham, P.D.J. Calcott, The structural and luminescence properties of porous silicon, J. Appl. Phys. 82 (1997) 909–965. doi:10.1063/1.366536.

[11] T. Schmidt, A.I. Chizhik, A.M. Chizhik, K. Potrick, A.J. Meixner, F. Huisken, Radiative exciton recombination and defect luminescence observed in single silicon nanocrystals, Phys. Rev. B. 86 (2012) 125302. doi:10.1103/PhysRevB.86.125302.

[12] S. Mann, Self-assembly and transformation of hybrid nano-objects and nanostructures under equilibrium and non-equilibrium conditions, Nat. Mater. 8 (2009) 781–792. doi:10.1038/nmat2496.

[13] L.H. Yu, C.D. Zangmeister, J.G. Kushmerick, Origin of Discrepancies in Inelastic Electron Tunneling Spectra of Molecular Junctions, Phys. Rev. Lett. 98 (2007) 206803. doi:10.1103/PhysRevLett.98.206803.

[14] J.E. Macdonald, M. Bar Sadan, L. Houben, I. Popov, U. Banin, Hybrid nanoscale inorganic cages, Nat. Mater. 9 (2010) 810–815. doi:10.1038/nmat2848.

[15] S. Su, X. Wei, Y. Zhong, Y. Guo, Y. Su, Q. Huang, S.-T. Lee, C. Fan, Y. He, Silicon Nanowire-Based Molecular Beacons for High-Sensitivity and Sequence-Specific DNA

Multiplexed Analysis, ACS Nano. 6 (2012) 2582–2590. doi:10.1021/nn2050449.

[16] K.-Q. Peng, S.-T. Lee, Silicon nanowires for photovoltaic solar energy conversion, Adv. Mater. Deerfield Beach Fla. 23 (2011) 198–215. doi:10.1002/adma.201002410.

[17] M. Lv, S. Su, Y. He, Q. Huang, W. Hu, D. Li, C. Fan, S.-T. Lee, Long-Term Antimicrobial Effect of Silicon Nanowires Decorated with Silver Nanoparticles, Adv. Mater. 22 (2010) 5463–5467. doi:10.1002/adma.201001934.

[18] J.S. Biteen, N.S. Lewis, H.A. Atwater, H. Mertens, A. Polman, Spectral tuning of plasmon-enhanced silicon quantum dot luminescence, Appl. Phys. Lett. 88 (2006) 131109. doi:10.1063/1.2191411.

[19] J. Goffard, D. Gérard, P. Miska, A.-L. Baudrion, R. Deturche, J. Plain, Plasmonic engineering of spontaneous emission from silicon nanocrystals, Sci. Rep. 3 (2013) 2672. doi:10.1038/srep02672.

[20] M.S. Dresselhaus, I.L. Thomas, Alternative energy technologies, Nature. 414 (2001) 332–337. doi:10.1038/35104599.

[21] J. Potočnik, Renewable Energy Sources and the Realities of Setting an Energy Agenda, Science. 315 (2007) 810–811. doi:10.1126/science.1139086.

[22] M. Grätzel, Photoelectrochemical cells, Nature. 414 (2001) 338–344. doi:10.1038/35104607.

[23] N.S. Lewis, D.G. Nocera, Powering the planet: chemical challenges in solar energy utilization, Proc. Natl. Acad. Sci. U. S. A. 103 (2006) 15729–15735. doi:10.1073/pnas.0603395103.

[24] M.A. Green, Recent developments in photovoltaics, Sol. Energy. 76 (2004) 3–8. doi:10.1016/S0038-092X(03)00065-3.

[25] E.A. Alsema, Energy pay-back time and CO2 emissions of PV systems, Prog. Photovolt. Res. Appl. 8 (2000) 17–25. doi:10.1002/(SICI)1099-159X(200001/02)8:1<17::AID-PIP295>3.0.CO;2-C.

[26] B.M. Kayes, H.A. Atwater, N.S. Lewis, Comparison of the device physics principles of planar and radial p-n junction nanorod solar cells, J. Appl. Phys. 97 (2005) 114302. doi:10.1063/1.1901835.

[27] E. Garnett, P. Yang, Light Trapping in Silicon Nanowire Solar Cells, Nano Lett. 10 (2010) 1082–1087. doi:10.1021/nl100161z.

[28] K.-Q. Peng, X. Wang, X.-L. Wu, S.-T. Lee, Platinum Nanoparticle Decorated Silicon Nanowires for Efficient Solar Energy Conversion, Nano Lett. 9 (2009) 3704–3709. doi:10.1021/nl901734e.

[29] F. Vietmeyer, B. Seger, P.V. Kamat, Anchoring ZnO Particles on Functionalized Single Wall Carbon Nanotubes. Excited State Interactions and Charge Collection, Adv. Mater. 19 (2007) 2935–2940. doi:10.1002/adma.200602773.

[30] G.M.A. Rahman, D.M. Guldi, E. Zambon, L. Pasquato, N. Tagmatarchis, M. Prato, Dispersable Carbon Nanotube/Gold Nanohybrids: Evidence for Strong Electronic Interactions, Small. 1 (2005) 527–530. doi:10.1002/smll.200400146.

[31] K.S. Leschkies, R. Divakar, J. Basu, E. Enache-Pommer, J.E. Boercker, C.B. Carter, U.R. Kortshagen, D.J. Norris, E.S. Aydil, Photosensitization of ZnO Nanowires with CdSe Quantum Dots for Photovoltaic Devices, Nano Lett. 7 (2007) 1793–1798. doi:10.1021/nl070430o.

[32] S. Chellammal, S. Manivannan, Determination of Quantum Confinement Effect of Nanoparticles, Adv. Mater. Res.

1051 (2014) 17–20. doi:10.4028/www.scientific.net/AMR.1051.17.

[33] J.P. Wilcoxon, P.P. Newcomer, G.A. Samara, Strong quantum confinement effects in semiconductors: FeS2 nanoclusters, Solid State Commun. 98 (1996) 581–585. doi:10.1016/0038-1098(95)00822-5.

[34] K.-Q. Peng, X. Wang, X.-L. Wu, S.-T. Lee, Platinum Nanoparticle Decorated Silicon Nanowires for Efficient Solar Energy Conversion, Nano Lett. 9 (2009) 3704–3709. doi:10.1021/nl901734e.

[35] Y. Su, X. Wei, F. Peng, Y. Zhong, Y. Lu, S. Su, T. Xu, S.-T. Lee, Y. He, Gold Nanoparticles-Decorated Silicon Nanowires as Highly Efficient Near-Infrared Hyperthermia Agents for Cancer Cells Destruction, Nano Lett. 12 (2012) 1845–1850. doi:10.1021/nl204203t.

[36] S.K. Ghosh, T. Pal, Interparticle Coupling Effect on the Surface Plasmon Resonance of Gold Nanoparticles: From Theory to Applications, Chem. Rev. 107 (2007) 4797–4862. doi:10.1021/cr0680282.

[37] M.M. Alvarez, J.T. Khoury, T.G. Schaaff, M.N. Shafigullin, I. Vezmar, R.L. Whetten, Optical Absorption Spectra of Nanocrystal Gold Molecules, J. Phys. Chem. B. 101 (1997) 3706–3712. doi:10.1021/jp962922n.

[38] L.A. Lyon, D.J. Peña, M.J. Natan, Surface Plasmon Resonance of Au Colloid-Modified Au Films: Particle Size Dependence, J. Phys. Chem. B. 103 (1999) 5826–5831. doi:10.1021/jp984739v.

[39] S. Link, M.A. El-Sayed, Spectral Properties and Relaxation Dynamics of Surface Plasmon Electronic Oscillations in Gold and Silver Nanodots and Nanorods, J. Phys. Chem. B. 103 (1999) 8410–8426. doi:10.1021/jp9917648.

[40] R.H. Ritchie, Plasma Losses by Fast Electrons in Thin Films, Phys. Rev. 106 (1957) 874–881. doi:10.1103/PhysRev.106.874.

[41] W.L. Barnes, A. Dereux, T.W. Ebbesen, Surface plasmon subwavelength optics, Nature. 424 (2003) 824–830. doi:10.1038/nature01937.

[42] http://www.annualreviews.org/doi/pdf/10.1146/annurev.physchem.58.032806.104607, http://www.annualreviews.org/doi/pdf/10.1146/annurev.physchem.58.032806.104607, (n.d.). http://www.annualreviews.org/doi/pdf/10.1146/annurev.physchem.58.032806.104607 (accessed June 7, 2016).

[43] J.J. Storhoff, R. Elghanian, R.C. Mucic, C.A. Mirkin, R.L. Letsinger, One-Pot Colorimetric Differentiation of Polynucleotides with Single Base Imperfections Using Gold Nanoparticle Probes, J. Am. Chem. Soc. 120 (1998) 1959–1964. doi:10.1021/ja972332i.

[44] R. Elghanian, J.J. Storhoff, R.C. Mucic, R.L. Letsinger, C.A. Mirkin, Selective colorimetric detection of polynucleotides based on the distance-dependent optical properties of gold nanoparticles, Science. 277 (1997) 1078–1081. doi: 10.1126/science.277.5329.1078

[45] R.P.V. Duyne, J.C. Hulteen, D.A. Treichel, Atomic force microscopy and surface-enhanced Raman spectroscopy. I. Ag island films and Ag film over polymer nanosphere surfaces supported on glass, J. Chem. Phys. 99 (1993) 2101–2115. doi:10.1063/1.465276.

[46] M. Duval Malinsky, K.L. Kelly, G.C. Schatz, R.P. Van Duyne, Nanosphere Lithography: Effect of Substrate on the Localized Surface Plasmon Resonance Spectrum of Silver Nanoparticles, J. Phys. Chem. B. 105 (2001) 2343–2350. doi:10.1021/jp002906x.

[47] W.W. Duley, Evidence for hydrogenated amorphous carbon in the Red Rectangle, Mon. Not. R. Astron. Soc. 215 (1985) 259–263. doi:10.1093/mnras/215.2.259.

[48] T.L. Smith, A.N. Witt, The Photophysics of the Carrier of Extended Red Emission, Astrophys. J. 565 (2002) 304. doi:10.1086/324542.

[49] http://micro.magnet.fsu.edu/primer/java/reflection/specular/,http://micro.magnet.fsu.edu/primer/java/reflection/specular/,(n.d.).http://micro.magnet.fsu.edu/primer/java/reflection/specular/ (accessed June 7, 2016).

[50] A.B. Murphy, Band-gap determination from diffuse reflectance measurements of semiconductor films, and application to photoelectrochemical water-splitting, Sol. Energy Mater. Sol. Cells. 91 (2007) 1326–1337. doi:10.1016/j.solmat.2007.05.005.

[51] J.M.F. Rodríguez, J.A.F. Fernández, Application of the second derivative of the Kubelka–Munk function to the semiquantitative analysis of Roman paintings, Color Res. Appl. 30 (2005) 448–456. doi:10.1002/col.20157.

[52] P. Kubelka, New Contributions to the Optics of Intensely Light-Scattering Materials. Part I, JOSA. 38 (1948) 448–457. doi:10.1364/JOSA.38.000448.

[53] S. Sakthivel, H. Kisch, Daylight Photocatalysis by Carbon-Modified Titanium Dioxide, Angew. Chem. Int. Ed. 42 (2003) 4908–4911. doi:10.1002/anie.200351577.

[54] S.J. Hong, S. Lee, J.S. Jang, J.S. Lee, Heterojunction BiVO4/WO3 electrodes for enhanced photoactivity of water oxidation, Energy Environ. Sci. 4 (2011) 1781–1787. doi:10.1039/C0EE00743A.

[55] L.J. Pilione, K. Vedam, J.E. Yehoda, R. Messier, P.J. McMarr, Thickness dependence of optical gap and void

fraction for sputtered amorphous germanium, Phys. Rev. B. 35 (1987) 9368–9371. doi:10.1103/PhysRevB.35.9368.

[56] S. Datta, K.L. Narasimhan, Model for optical absorption in porous silicon, Phys. Rev. B. 60 (1999) 8246–8252. doi:10.1103/PhysRevB.60.8246.

[57] Z.R. Smith, R.L. Smith, S.D. Collins, Mechanism of nanowire formation in metal assisted chemical etching, Electrochimica Acta. 92 (2013) 139–147. doi:10.1016/j.electacta.2012.12.075.

[58] A. Backes, A. Bittner, M. Leitgeb, U. Schmid, Influence of metallic catalyst and doping level on the metal assisted chemical etching of silicon, Scr. Mater. 114 (2016) 27–30. doi:10.1016/j.scriptamat.2015.11.014.

[59] A.E. Miroshnichenko, S. Flach, Y.S. Kivshar, Fano resonances in nanoscale structures, Rev. Mod. Phys. 82 (2010) 2257–2298. doi:10.1103/RevModPhys.82.2257.

[60] K.W. Kolasinski, Electron transfer during metal-assisted and stain etching of silicon, Semicond. Sci. Technol. 31 (2016) 14002. doi:10.1088/0268-1242/31/1/014002.

[61] N. Geyer, B. Fuhrmann, Z. Huang, J. de Boor, H.S. Leipner, P. Werner, Model for the Mass Transport during Metal-Assisted Chemical Etching with Contiguous Metal Films As Catalysts, J. Phys. Chem. C. 116 (2012) 13446–13451. doi:10.1021/jp3034227.

[62] K. Balasundaram, J.S. Sadhu, J.C. Shin, B. Azeredo, D. Chanda, M. Malik, K. Hsu, J.A. Rogers, P. Ferreira, S. Sinha, X. Li, Porosity control in metal-assisted chemical etching of degenerately doped silicon nanowires, Nanotechnology. 23 (2012) 305304. doi:10.1088/0957-4484/23/30/305304.

[63] A.M. Alwan, A.J. Hayder, A.A. Jabbar, Study on morphological and structural properties of silver plating on

laser etched silicon, Surf. Coat. Technol. 283 (2015) 22–28. doi:10.1016/j.surfcoat.2015.10.037.

[64] Y. Qi, Z. Wang, M. Zhang, F. Yang, X. Wang, A Processing Window for Fabricating Heavily Doped Silicon Nanowires by Metal-Assisted Chemical Etching, J. Phys. Chem. C. 117 (2013) 25090–25096. doi:10.1021/jp407720e.

[65] H.S. Mavi, S. Prusty, M. Kumar, R. Kumar, A.K. Shukla, S. Rath, Formation of Si and Ge quantum structures by laser-induced etching, Phys. Status Solidi -Appl. Mater. Sci. 203 (2006) 2444–2450. doi:10.1002/pssa.200521027.

[66] R. Kumar, H.S. Mavi, A.K. Shukla, Macro and microsurface morphology reconstructions during laser-induced etching of silicon, Micron. 39 (2008) 287–293. doi:10.1016/j.micron.2007.04.005.

[67] Z. Huang, N. Geyer, P. Werner, J. de Boor, U. Gösele, Metal-Assisted Chemical Etching of Silicon: A Review, Adv. Mater. 23 (2011) 285–308. doi:10.1002/adma.201001784.

[68] G.K. Darbha, A. Ray, P.C. Ray, Gold Nanoparticle-Based Miniaturized Nanomaterial Surface Energy Transfer Probe for Rapid and Ultrasensitive Detection of Mercury in Soil, Water, and Fish, ACS Nano. 1 (2007) 208–214. doi:10.1021/nn7001954.

[69] N. Ma, J. Yang, K.M. Stewart, S.O. Kelley, DNA-Passivated CdS Nanocrystals: Luminescence, Bioimaging, and Toxicity Profiles, Langmuir. 23 (2007) 12783–12787. doi:10.1021/la7017727.

[70] J. Zheng, F. Huang, S. Yin, Y. Wang, Z. Lin, X. Wu, Y. Zhao, Correlation between the Photoluminescence and Oriented Attachment Growth Mechanism of CdS Quantum

Dots, J. Am. Chem. Soc. 132 (2010) 9528–9530. doi:10.1021/ja101848w.

[71] H. Tang, C. Liu, H. He, Surface plasmon enhanced photoluminescence from porous silicon nanowires decorated with gold nanoparticles, RSC Adv. 6 (2016) 59395–59399. doi:10.1039/C6RA06019F.

[72] M.V. Wolkin, J. Jorne, P.M. Fauchet, G. Allan, C. Delerue, Electronic States and Luminescence in Porous Silicon Quantum Dots: The Role of Oxygen, Phys. Rev. Lett. 82 (1999) 197–200. doi:10.1103/PhysRevLett.82.197.

[73] K. Potrick, F. Huisken, Photoluminescence properties of silicon nanocrystals interacting with gold nanoparticles via exciton-plasmon coupling, Phys. Rev. B. 91 (2015) 125306. doi:10.1103/PhysRevB.91.125306.

[74] H. Sugimoto, T. Chen, R. Wang, M. Fujii, B.M. Reinhard, L. Dal Negro, Plasmon-Enhanced Emission Rate of Silicon Nanocrystals in Gold Nanorod Composites, ACS Photonics. 2 (2015) 1298–1305. doi:10.1021/acsphotonics.5b00233.

[75] J.S. Biteen, L.A. Sweatlock, H. Mertens, N.S. Lewis, A. Polman, H.A. Atwater, Plasmon-Enhanced Photoluminescence of Silicon Quantum Dots: Simulation and Experiment, J. Phys. Chem. C. 111 (2007) 13372–13377. doi:10.1021/jp074160+.

[76] E. Sakat, I. Bargigia, M. Celebrano, A. Cattoni, S. Collin, D. Brida, M. Finazzi, C. D'Andrea, P. Biagioni, Time-Resolved Photoluminescence in Gold Nanoantennas, ACS Photonics. (2016). doi:10.1021/acsphotonics.6b00039.

[77] L. Stalmans, J. Poortmans, H. Bender, M. Caymax, K. Said, E. Vazsonyi, J. Nijs, R. Mertens, Porous silicon in crystalline silicon solar cells: a review and the effect on the internal quantum efficiency, Prog. Photovolt. Res. Appl. 6

(1998) 233–246. doi:10.1002/(SICI)1099-159X(199807/08)6:4<233::AID-PIP207>3.0.CO;2-D.

[78] S.K. Srivastava, D. Kumar, P.K. Singh, M. Kar, V. Kumar, M. Husain, Excellent antireflection properties of vertical silicon nanowire arrays, Sol. Energy Mater. Sol. Cells. 94 (2010) 1506–1511. doi:10.1016/j.solmat.2010.02.033.

[79] K.A. Salman, K. Omar, Z. Hassan, The effect of etching time of porous silicon on solar cell performance, Superlattices Microstruct. 50 (2011) 647–658. doi:10.1016/j.spmi.2011.09.006.

[80] S. Pillai, K.R. Catchpole, T. Trupke, M.A. Green, Surface plasmon enhanced silicon solar cells, J. Appl. Phys. 101 (2007) 93105. doi:10.1063/1.2734885.